TURBULENT DRAG REDUCTION VIA TRANSVERSE WALL OSCILLATIONS: EVALUATION OF ACTIVE AND PASSIVE APPROACHES

Michael P. Whitmore
Center for Turbulence Research
Stanford University
488 Escondido Mall, Stanford, CA, USA
mpw2@stanford.edu

M. Godfrey Mungal
Department of Mechanical Engineering
Santa Clara University
Santa Clara, CA, USA
mgmungal@scu.edu

ABSTRACT

The reduction of turbulent drag via transverse wall oscillations has been demonstrated as a robust drag reduction mechanism by both experiments and high-fidelity simulations. This mechanism has been demonstrated by active means, both for temporal wall oscillations and traveling-wave wall oscillations. In this work, wall-modeled large-eddy simulation (WMLES) is used to simulate this drag reduction mechanism and is subsequently validated against available data. WMLES of oscillating pipes is first used to study the case of active drag reduction. WMLES is then used to evaluate the potential for passive drag reduction by inducing the drag reducing effects of transverse wall oscillations through geometric modifications of pipes. A slight drag reduction effect is observed for a small range of twist amplitudes across three different cross-sectional geometries. For larger twist amplitudes, the geometry modifications increase the drag relative to a round pipe.

INTRODUCTION

The reduction of turbulent drag in pipes has the potential to lead to substantial cost savings in a number of engineering applications, one such example being pipelines which require pumps to overcome the effects of drag over long distances. Turbulent drag reduction has been demonstrated through a number of approaches, such as riblets and injection of polymers; however, these methods also come with drawbacks. Notably, riblets can be difficult to manufacture and only reduce drag at a narrow set of flow conditions, while polymers can degrade over time and require re-injection into the flow to maintain the drag reducing effect.

Transverse wall oscillations have recently been shown to be a drag reduction mechanism that is robust to a range of flow conditions while also not requiring introduction of depletable materials.

Marusic *et al.* (2021) used a mix of experiments and simulations to demonstrate the effect of transverse traveling-wave wall oscillations induced by a number of moving panels. The results showed drag reduction up to 25% with a net reduction in power for some Reynolds numbers.

Sabidussi *et al.* (2024) performed experiments of an azimuthally oscillating pipe where drag reduction of up to 31% was demonstrated and the drag reduction mechanism was shown to be largely Reynolds number independent for a range of conditions.

COMPUTATIONAL FRAMEWORK

The code used to perform the WMLES of the pipes in this work is charLES, which is a 2nd-order, low-dissipation, unstructured finite-volume code for compressible ideal gas flow from Cadence Design Systems. While the code used is for compressible flow, the simulations are run at low Mach numbers such that the effects of compressibility are negligible to approximate incompressible flow. The code uses Voronoi-based mesh generation which can easily generate body-fitted meshes for complex geometries (Brès *et al.*, 2018).

TEMPORALLY-OSCILLATING PIPE

The case of an azimuthally oscillating wall turbulent pipe is simulated in order to validate the LES against results in the literature. The case simulated is a circular pipe with an length of 12.5 diameters and periodic boundary conditions in the axial direction. The bulk Reynolds number of the pipe is $Re_b = 11700$ based on the pipe diameter which corresponds to a friction Reynolds number of $Re_\tau \approx 366$. The wall of the pipe is oscillated in the azimuthal direction at varying rotational speed amplitudes with a non-dimensional oscillation period $T^+ = 100$. The non-dimensional azimuthal accelerations of the pipe range from $a^+ \approx 0.06$ to 0.30.

The grid resolution of these simulations is chosen such that, near the center of the pipe, the largest control volume spacings are approximately 0.05 pipe diameters. The grid is isotropically refined close to the walls of the pipe such that the most refined control volume spacings near the pipe wall are approximately 0.0063 pipe diameters. This grid resolution is chosen as the baseline and leads to approximately 15.4 million control volumes in total.

The axial drag reduction predictions of the WMLES of the oscillating pipe are shown in Figure 1 and compared to the experiments of Choi & Graham (1998) and Sabidussi *et al.* (2024). Because the friction Reynolds number of the WMLES cases is relatively low, the WMLES data is clustered towards the right half of the plot. For the lowest value of the non-dimensional acceleration, the LES agrees closely with the experimental values of drag reduction. For the higher values of non-dimensional acceleration, the LES shows a similar trend to the experiments but has slightly higher drag reduction compared to the experimental results. The results show a generally good agreement between the WMLES and the experimental results in the literature which suggests that the simulations are capable of capturing the important drag reducing mechanisms in this flow configuration. This validates the approach such that it can be used to evaluate previously unstudied geometries in a predictive manner.

GEOMETRICALLY-INDUCED AZIMUTHAL OSCILLATION

In this section, various shapes are explored in order to determine the feasibility of inducing the azimuthally oscillating wall drag reduction mechanism through passive means. The geometries are evaluated using the WMLES approach that was validated against reference data in the previous section.

Three cross-sectional shapes are chosen, which include a regular polygon, an inverted regular polygon, and a so-called "cactus" shape. The cactus shape is reminiscent of designs of riblets (particularly similar to the sinusoidal riblets studied by Peet *et al.* (2008)); however, the scale of the ridge shapes is not determined by an inner unit scaling with Reynolds number and is instead a large-scale geometric structure.

In order to allow easier comparison between these shapes and a circular pipe, the cross-sections are all scaled such that they have a common hydraulic diameter, defined as $D_H = 4A/P$, where A is the cross-sectional area and P is the perimeter. The common choice of hydraulic diameter allows the shapes to be simulated with the same bulk Reynolds number $Re_b = U_b D_H/\nu = 11700$, where U_b is the prescribed bulk velocity and ν is the kinematic viscosity. The three cross section shapes are plotted in Figure 2(a-c).

Along the axial direction of these pipes, a sinusoidal twist is applied to the cross section to attempt to induce some azimuthal rotation to the flow near the wall. In the present geometries, over the length of the domain, $12.5D_H$, exactly one full period of oscillation is applied. In order to vary the amount of rotation the flow will undergo, the amplitude of the twist, ϕ_c, is varied across the three geometries, from 0.15 up to 2.4 radians. Larger twist amplitudes attempt to rotate the flow near the wall more aggressively. An example of a pipe with twist amplitude of 0.6 radians is shown in Figure 2(d).

A sweep of WMLES calculations are performed for the three cross sections as well as for six different amounts of twist amplitude, which includes the zero twist case as a baseline. The resulting level of drag reduction (or increase) relative to the circular pipe case is plotted in Figure 3 as a ratio of friction Reynolds numbers over a range of twist amplitudes. Overall, there is a general trend observed that for a low level of twist amplitude, a slight drag reduction effect is realized, with the cactus shape showing a little less than $\sim 2\%$ reduction in drag relative to the circular pipe, and the other shapes showing less than 1% reduction. At higher levels of twist amplitude, the drag begins to increase relative to the circular pipe case. This is hypothesized to be caused by the flow failing to turn with the geometry at larger twist amplitudes and instead flowing over the twisting geometric features leading to a rise in pressure drag. This demonstrates that while it is possible to induce the oscillating wall drag reduction effect through these passive means, a careful balance is required to ensure that the flow follows the geometric features at the wall and does not flow over them as if they are a type of geometric roughness impeding the flow.

DISCUSSION

Among the three cross-sectional geometries tested, the cactus shape produced the most pronounced drag reduction effect; therefore, it will serve as the primary case for the remainder of the discussion. First, in order to further verify the WMLES results for the drag reduction in the cactus shape cross section, given the lack of reference results for this geometry, a grid refinement study is conducted. Following the best practice for the charLES code, further refined grids are generated by inserting layers of isotropically $2\times$ refined control volumes in layers near the boundary surface. A sequence of fine grid simulations ($2\times$ refined or 77 million control volumes) is performed at all twist amplitudes, as well as an additional extra fine grid simulation ($4\times$ refined or 322 million control volumes) at a single twist amplitude of 0.3 radians, coinciding with the most significant drag reduction. The extra fine grid simulation was only performed at a single twist amplitude due to the significant increase in computational cost for that case. The results of the grid refinement study on the drag reduction are plotted in Figure 4. While there is a discrepancy of approximately 1% of the smooth pipe drag between the baseline and the fine grid results, the qualitative behavior is unchanged, with the extra fine grid simulation showing even less discrepancy from the fine grid, suggesting the solution is suitably grid converged in order to investigate the drag reduction mechanism in this case.

In order to better understand the mechanism behind the drag reduction in the cactus-shaped pipe case, the temporally- and azimuthally-averaged skin friction is plotted along the axial coordinate of the pipe in Figure 5. These results are normalized by the average drag of the zero twist amplitude case. Viewing the averaged skin friction along the axial coordinate of the pipe highlights the areas of the pipe where drag is most significantly reduced (and increased) with respect to the zero twist case, which highlights the areas where the mechanism governing the drag reduction is likely to be most active. In the smaller twist amplitude cases of 0.15 and 0.3 radians, the friction velocity is approximately sinusoidal above and below the friction velocity of the zero twist case, but with a bias slightly below the zero twist case, showing the net drag reduction. In the 0.6 radian case, the friction velocity peak starts to increase, while a secondary peak starts to form, diminishing the overall drag reduction effect. By the 1.2 and 2.4 radian cases, the friction velocity peak becomes even more apparent while the troughs in the friction velocity remain the same or diminish in amplitude. To better understand the flow features that lead to these effects, the twist amplitude cases of $\phi_c = 0.3$ and $\phi_c = 2.4$ radians are chosen as baselines for a drag-reduced as well as a drag-increased case, respectively.

In order to investigate the mean flow structures in the cactus shape pipes, the flow field is averaged over time, as well as over the 12-fold azimuthal symmetry, and over the axial direction while adjusting for the phase of the pipe twist. The volume-averaged axial velocity is plotted in Figure 6(a,b) for the zero twist baseline and the 0.3 radian twist case. The 0.3 radian twist case shows a lack of secondary flow features which leads to a reduced velocity on average inside the troughs of the geometry, suggesting that the twisting of the surface geometry effectively disturbs the secondary flows to reduce the overall drag in the pipe. This is corroborated by the Reynolds shear stresses plotted in Figure 7(a,b) which show that the twisted case diffuses the Reynolds stress peaks away from the peaks of the geometry and ultimately reduces their peak value relative to the zero twist case. The azimuthal velocities shown in Figure 8(a,b) also show the diminished secondary flow from the zero twist case to the 0.3 radian twist case.

In contrast to the 0.3 radian twist case which shows the most significant drag reduction, the cases with increased twist amplitude start to show diminishing returns, ultimately leading to a significant increase in drag. The 2.4 radian twist case shows the largest increase in drag with an approximately 8% increase in drag over a round pipe. Figure 5 shows that while this case does maintain some regions of reduced drag, there are significant spikes which raise the drag overall. The Reynolds shear stress plotted in Figure 9(a) shows a localized peak that has moved inside of the troughs of the geometry. This is consistent with flow passing over the geometric features, rather than following their turning directions, mixing faster fluid into the troughs. The azimuthal velocity in Figure 9(b) shows that the secondary flow from the zero twist case has been effectively reversed, with azimuthal velocities in the mean flowing towards the low point of the trough. Ultimately, this results from the rapid turning of the geometric features at the higher twist amplitudes such that the flow near the wall is not able to follow, instead flowing over the geometric features and incurring an increased drag. This highlights the fact that the use of the surface geometry to control the flow must be selected carefully in order to balance the benefits of the drag reduction effect with the drag penalty incurred from trying to turn the flow too aggressively.

CONCLUSIONS

The drag reduction effect of a transverse oscillating wall has recently been shown through high fidelity simulations and experiments to be a robust drag reduction mechanism, with significant drag reduction at a range of Reynolds numbers. While this drag reduction effect is robust, the practical challenges of transverse oscillating walls and pipes make the active approach to this drag reduction effect unrealistic. Inducing this drag reduction effect passively by modifying the geometry of a pipe wall is desirable since it is easier to practically implement. First, WMLES calculations were carried out for the azimuthally-oscillating circular pipe and the results were used to validate the WMLES approach against experimental data. Secondly, three cross-sectional geometries were chosen to form pipes with twisting geometrical features in the axial direction to attempt to passively induce the oscillating wall effect in the flow closest to the wall.

The WMLES results for the three cross-sectional geometries show a slight drag reduction effect at low levels of axial twist amplitude. At higher levels of twist amplitude, the rotation of the geometrical features becomes too aggressive, such that the flow near the wall of these pipes begins to flow over the features rather than follow them, leading to a rise in pressure drag that raises the overall drag through the pipe. These results suggest that while some slight drag reduction effect may be attainable through the introduction of twisting geometric features at the pipe walls, there is a balance that must be maintained so that the pressure drag introduced by these geometric features does not begin to overwhelm the drag reduction effect.

Further analysis of the mean flow features of the cactus-shaped cross-section geometry showed that at lower twist amplitudes where a drag reduction is achieved, the flow induced by the turning geometry disturbs the secondary flows into the troughs, maintaining lower speed flow near the walls and reducing the peak Reynolds shear stresses in the mean. The reduction of the Reynolds shear stresses is consistent with the reduction of the turbulent part of the drag per the decomposition of Fukagata *et al.* (2002). For the higher twist amplitude cases where the drag begins to increase, the flow starts to pass over the ridges rather than follow them, leading to more mixing inside the troughs as well as a stronger, reversed secondary flow. This highlights the careful balance required to achieve a reduced drag while not attempting to force the flow past the point that it can smoothly follow the surface.

ACKNOWLEDGMENTS

M.P.W. acknowledges funding from the NASA Transformational Tools and Technologies project (grant no. 80NSSC20M0201). This research used resources of the Oak Ridge Leadership Computing Facility at the Oak Ridge National Laboratory, which is supported by the Office of Science of the U.S. Department of Energy under Contract No. DE-AC05-00OR22725.

REFERENCES

Brès, Guillaume A., Bose, Sanjeeb T., Emory, Michael, Ham, Frank E., Schmidt, Oliver T., Rigas, Georgios & Colonius, Tim 2018 Large-eddy simulations of co-annular turbulent jet using a voronoi-based mesh generation framework. In *2018 AIAA/CEAS Aeroacoustics Conference*, pp. AIAA 2018–3302.

Choi, Kwing-So & Graham, Mark 1998 Drag reduction of turbulent pipe flows by circular-wall oscillation. *Physics of Fluids* **10** (1), 7–9.

Fukagata, Koji, Iwamoto, Kaoru & Kasagi, Nobuhide 2002 Contribution of reynolds stress distribution to the skin friction in wall-bounded flows. *Physics of Fluids* **14** (11), L73–L76.

Marusic, I, Chandran, D, Rouhi, A, Fu, M K, Wine, D, Holloway, B, Chung, D & Smits, A 2021 An energy-efficient pathway to turbulent drag reduction. *Nature Communications* **12** (5805).

Peet, Yulia, Sagaut, Pierre & Charron, Yves 2008 Turbulent drag reduction using sinusoidal riblets with triangular cross-section. In *38th Fluid Dynamics Conference and Exhibit*, pp. AIAA 2008–3745.

Sabidussi, L F, Ding, L, Hultmark, M & Smits, A J 2024 Reducing drag in turbulent pipe flow by azimuthal wall oscillation. In *13th International Symposium on Turbulence and Shear Flow Phenomena (TSFP13)*. Montreal, Canada.

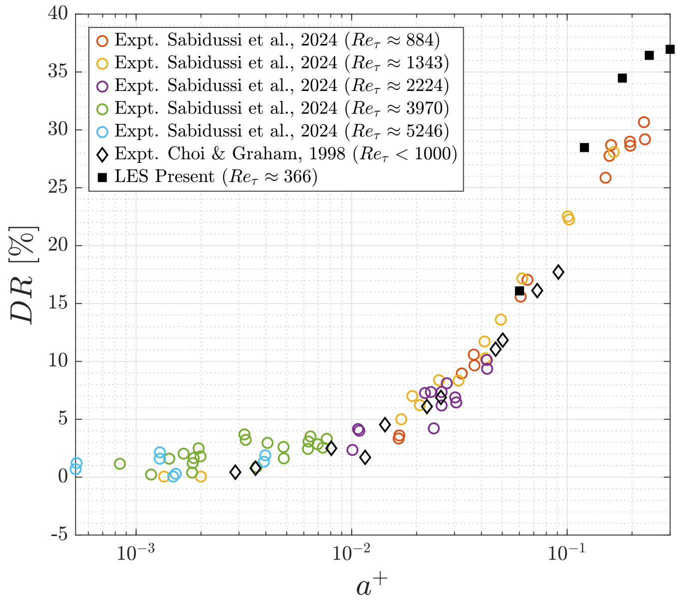

Figure 1. Drag reduction of the oscillating pipe plotted with respect to the non-dimensional acceleration. Present LES results are compared to experimental results of Choi & Graham (1998) and Sabidussi *et al.* (2024).

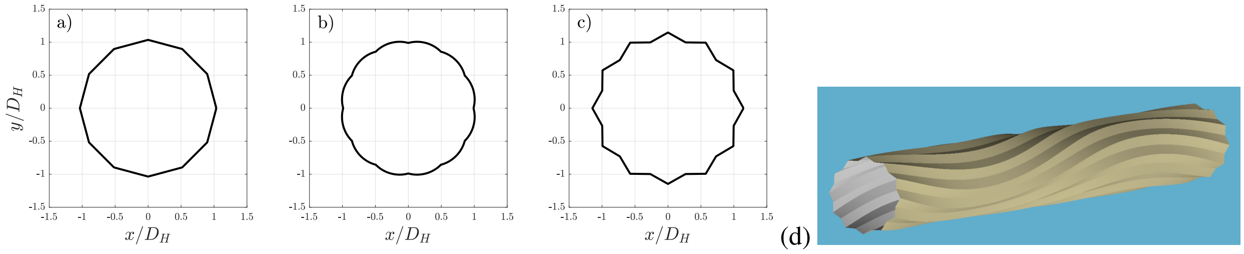

Figure 2. Shapes of the cross sections used for the aim of passive induction of the azimuthal flow oscillations. The (a) regular polygon, (b) inverted polygon, and (c) cactus shape are plotted with unit hydraulic diameters. (d) Oblique view of the cactus shape geometry with sinusoidal twist along the axial direction. This geometry shows a twist amplitude of 0.6 radians.

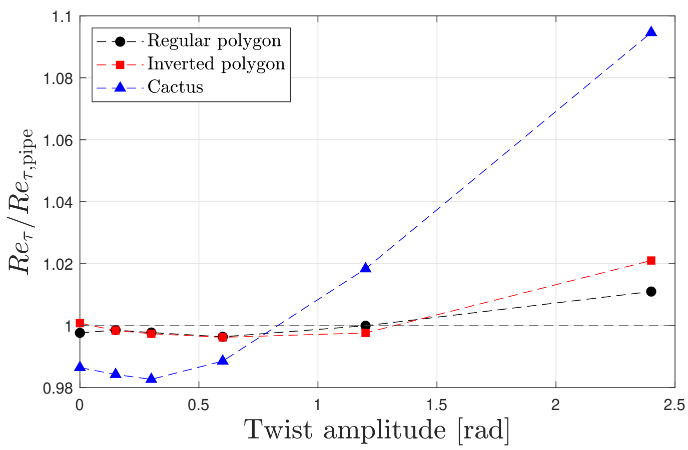

Figure 3. Change in drag (measured as friction Reynolds number) relative to a circular pipe of equal hydraulic diameter as a function of the twist amplitude for three cross-sectional geometries.

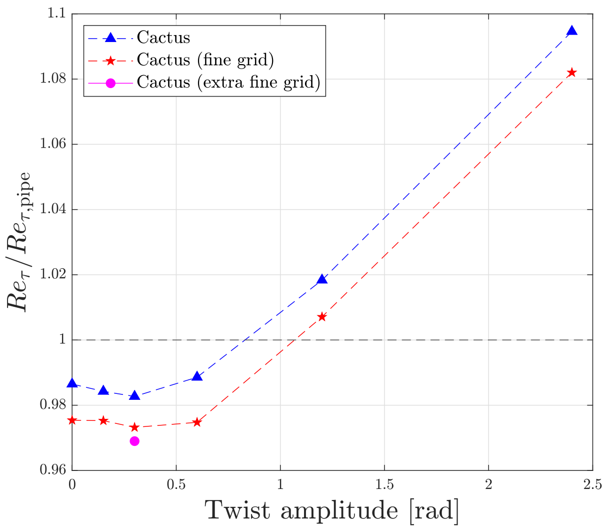

Figure 4. Grid refinement study of the drag reduction for the cactus shape geometry at varying twist amplitudes.

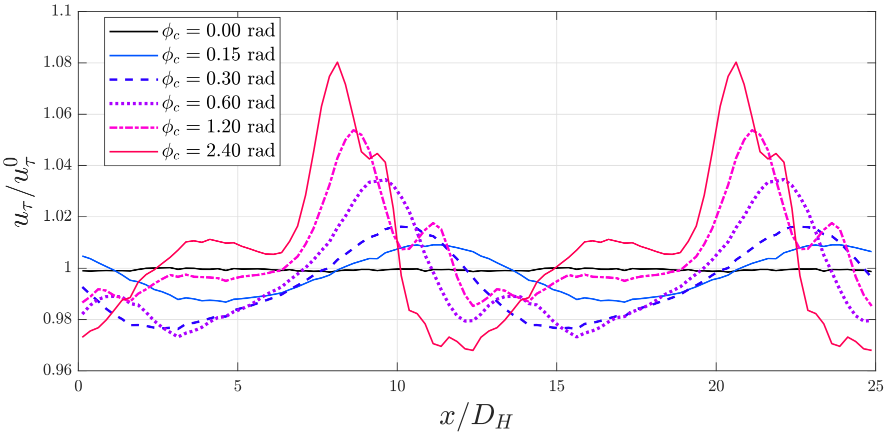

Figure 5. Azimuthally- and temporally-averaged friction velocity, u_τ, as a function of the axial coordinate in the cactus-shaped pipes with varying twist amplitudes, normalized by the average friction velocity of the zero twist case, u_τ^0.

(a) 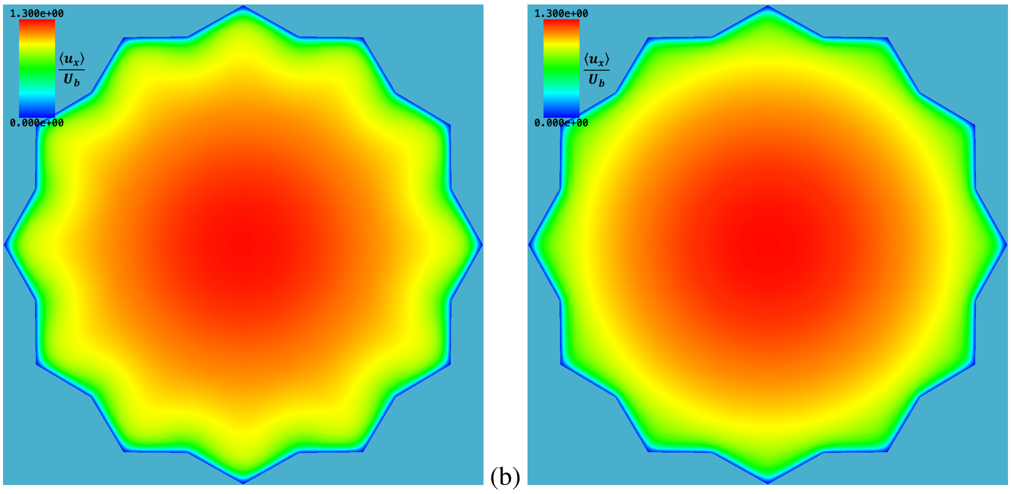 (b)

Figure 6. Volume-averaged axial velocity $\langle u_x \rangle$ for the (a) zero twist amplitude and (b) 0.3 radian twist amplitude cases.

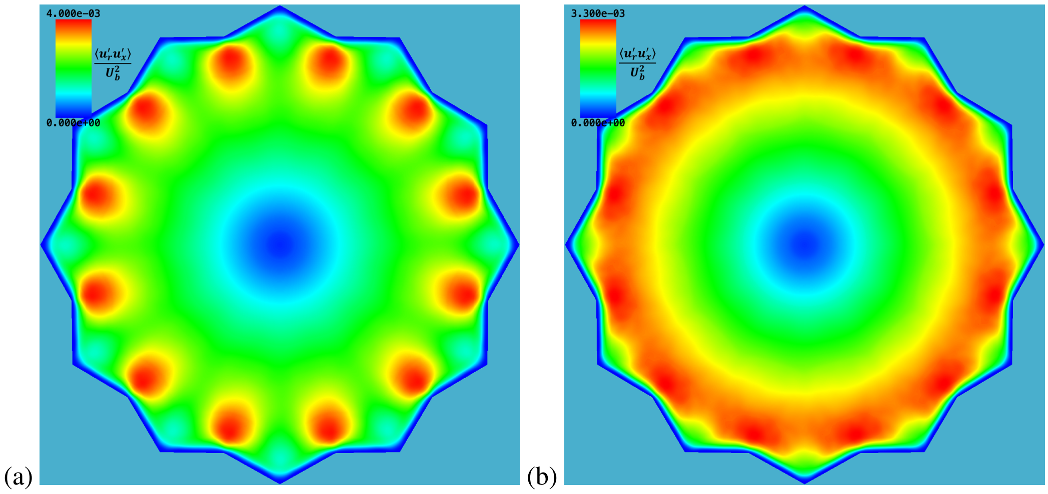

Figure 7. Volume-averaged Reynolds shear stress $\langle u_r' u_x' \rangle$ for the (a) zero twist amplitude and (b) 0.3 radian twist amplitude cases.

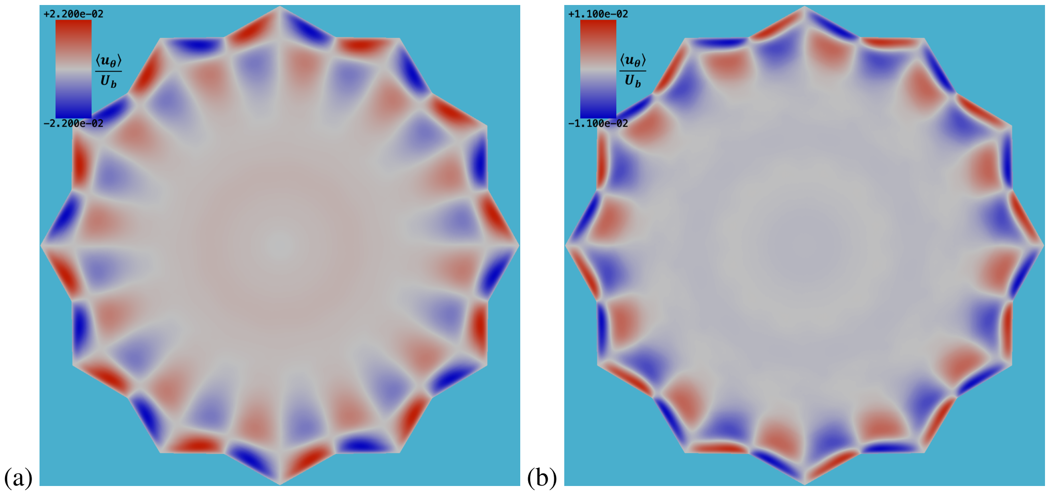

Figure 8. Volume-averaged azimuthal velocity $\langle u_\theta \rangle$ for the (a) zero twist amplitude and (b) 0.3 radian twist amplitude cases.

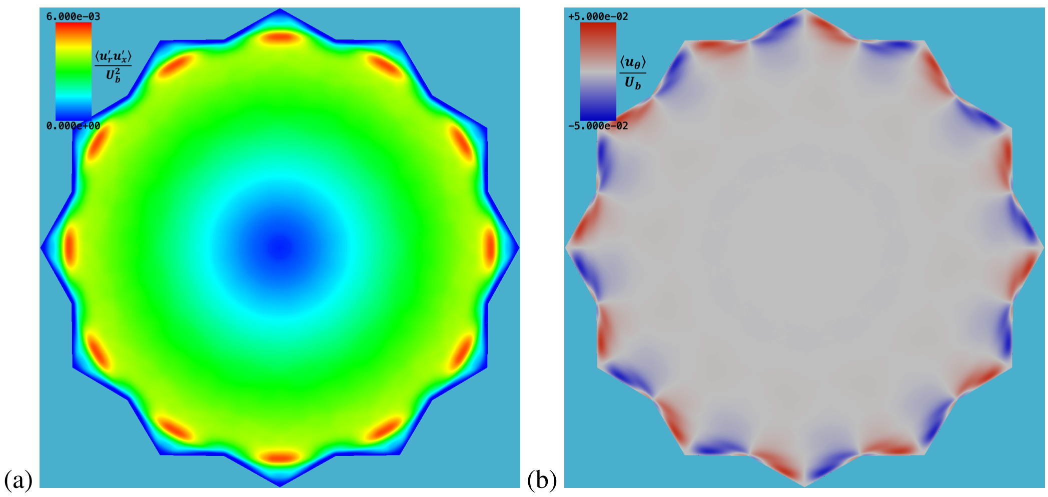

Figure 9. (a) Volume-averaged Reynolds shear stress $\langle u_r' u_x' \rangle$ and (b) volume-averaged azimuthal velocity $\langle u_\theta \rangle$ for the 2.4 radian twist case.